International Journal of Computer Vision 70(3), 231–240, 2006

DOI: 10.1007/s11263-006-6703-9

A Linear Image Reconstruction Framework Based on Sobolev Type Inner Products

BART JANSSEN*, FRANS KANTERS*, REMCO DUITS*, LUC FLORACK
AND BART TER HAAR ROMENY
Eindhoven University of Technology, Den Dolech 2, Postbus 513
5600 MB Eindhoven, The Netherlands
B.J.Janssen@tue.nl
F.M.W.Kanters@tue.nl
R.Duits@tue.nl
L.M.J.Florack@tue.nl
B.M.terHaarRomeny@tue.nl

Received May 27, 2005; Revised December 13, 2005; Accepted December 15, 2005

Abstract. Exploration of information content of features that are present in images has led to the development of several reconstruction algorithms. These algorithms aim for a reconstruction from the features that is visually close to the image from which the features are extracted. Degrees of freedom that are not fixed by the constraints are disambiguated with the help of a so-called prior (i.e. a user defined model). We propose a linear reconstruction framework that generalizes a previously proposed scheme. The algorithm greatly reduces the complexity of the reconstruction process compared to non-linear methods. As an example we propose a specific prior and apply it to the reconstruction from singular points. The reconstruction is visually more attractive and has a smaller $\mathbb{L}_2$-error than the reconstructions obtained by previously proposed linear methods.

Keywords: reconstruction; scale space; sampling; deep structure

1. Introduction

Reconstruction from differential structure of scale space interest points was first introduced by Nielsen and Lillholm (2001). Using the reconstruction the information content of these points can be investigated. Unser and Aldroubi (1994) generalized sampling theory by Shannon (1949) and Papoulis (1977) by finding a consistent reconstruction of a signal from its integer shifted filter responses, i.e. a reconstruction that is indistinguishable from its original when observed through the filters the features were extracted with. The consistency requirement is adopted by Lillholm et al. (2003) Nielsen and Lillholm (2001) and Kybic et al. (2001, 2002). They describe a variational framework that finds a consistent reconstruction that minimizes a so called prior (i.e. a user defined model). The disadvantage of this variational approach is that the reconstruction algorithm is not linear and therefore slow and somewhat cumbersome to implement. Kanters et al. (2003) investigated a special case of the reconstruction by Nielsen and Lillholm (2001) by adopting the $\mathbb{L}_2$-norm as a prior. We shall refer to this as the *standard linear reconstruction scheme*. Advantages of this approach are that the reconstruction algorithm is linear and analytical results for the generalized correlation matrix can be found. The disadvantage is

*Bart Jansen, Frans Kanters and Remco Duits are joint main authors of this article.

that this method is qualitatively outperformed by non-linear reconstruction methods (Lillholm et al., 2003; Kybic et al., 2002; Nielsen and Lillholm, 2001).

We propose a general reconstruction framework which can be applied to a large set of priors. Any prior that can be described by a norm formed by an inner product can be mapped to this framework. Our method overcomes the disadvantages of the standard linear reconstruction scheme by Kanters et al. (2003) while retaining linearity. This is done by replacing the $\mathbb{L}_2$-inner product by an inner product of Sobolev type. To verify the proposed method we apply it to the reconstruction from singular points. A prior that smoothens the reconstructed image is selected. This results in a reconstruction that has as few additional singular points as possible under the constraints. Also the features are enriched by taking higher order derivatives into account.

For a mathematically rigorous analysis of linear image reconstruction and its connection to Gelfand triples we refer to Duits (2005), Section 3.4.

2. Theory

Definition 1 ($\mathbb{L}_2$-Inner Product). The $\mathbb{L}_2 - inner$ product for f, g $\in \mathbb{L}_2(\mathbb{R}^2)$ *is given by*

$$(f, g)_{\mathbb{L}_2} = \int_{\mathbb{R}^2} \overline{f(x)}\, g(x) dx. \tag{1}$$

This is the standard inner product used in previous work (Kanters et al., 2003; Lillholm et al., 2003; Nielsen and Lillholm, 2001).

The reconstruction problem boils down to the selection of an instance of the metameric class consisting of $g \in \mathbb{L}_2(\mathbb{R}^2)$ such that

$$(\psi_i, g)_{\mathbb{L}_2} = c_i, \quad (i = 1 \ldots N) \tag{2}$$

with ψ_i denoting the distinct localized filters that generate the ith filter response $c_i = (\psi_i, f)_{\mathbb{L}_2} \in \mathbb{C}$, i.e. the selection from the equivalence class of images g that share the same predefined set of features (2). The selection of g is done by minimizing a prior subject to the constraints of equation (2). A distinction can be made between priors (global constraints) that are constructed by a norm formed by an inner product and those that are constructed by a norm that is not formed by an inner product. In the former case it is possible to translate the reconstruction problem to a linear projection. This maps the reconstruction problem onto straightforward linear algebra. To this end we propose a generalization of Definition 1 as follows.

Definition 2 (A-Inner Product). We define A to be an operator on $\mathbb{L}_2(\mathbb{R}^2)$ such that $(I + A^\dagger A)^{-1}$ is bounded[1]. Then

$$(f, g)_A = (f, g)_{\mathbb{L}_2} + (Af, Ag)_{\mathbb{L}_2}. \tag{3}$$

Note that we can write

$$(f, g)_A = (f, (I + A^\dagger A)g)_{\mathbb{L}_2}. \tag{4}$$

For an image $f \in \mathbb{L}_2(\mathbb{R}^2)$ we consider a collection of filters $\psi_i \in \mathbb{L}_2(\mathbb{R}^2)$ and filter responses $c_i, i = 1, \ldots, N$, given by

$$c_i = (\psi_i, f)_{\mathbb{L}_2}. \tag{5}$$

Thus the a priori known features are given in terms of an $\mathbb{L}_2$-inner product. In order to express these features relative to the new inner product we seek an effective filter, κ_i say, such that

$$(\kappa_i, f)_A = (\psi_i, f)_{\mathbb{L}_2} \tag{6}$$

for all f. We will henceforth refer to ψ_i as an "$\mathbb{L}_2$-filter" and to κ_i as its corresponding "A-filter".

Lemma 1 (A-Filters). *Given $\psi_i \in \mathbb{L}_2(\mathbb{R}^2)$ then its corresponding A-filter is given by*

$$\kappa_i = (I + A^\dagger A)^{-1} \psi_i. \tag{7}$$

Applying Definition 2,

$$\begin{aligned}(\kappa_i, f)_A &= \left((I + A^\dagger A)^{-1}\psi_i, f\right)_A \\ &= \left((I + A^\dagger A)(I + A^\dagger A)^{-1}\psi_i, f\right)_{\mathbb{L}_2} \\ &= (\psi_i, f)_{\mathbb{L}_2}. \end{aligned} \tag{8}$$

We aim to establish a reconstruction g that satisfies equation (2) and minimizes

$$E(g) = \frac{1}{2}(g, g)_A. \tag{9}$$

Since g satisfies equation (2) we may as well write

$$E(g) = \frac{1}{2}((g, g)_{\mathbb{L}_2} + (Ag, Ag)_{\mathbb{L}_2}) - \lambda^i((\psi_i, g)_{\mathbb{L}_2} - c_i), \tag{10}$$

in other words

$$E(g) = \frac{1}{2}(g, g)_A - \lambda^i ((\kappa_i, g)_A - c_i). \tag{11}$$

Einstein summation convention applies to upper and lower feature indices $i = 1...N$, i.e. whenever an upper index matches a lower one it is supposed to be regarded as a dummy summation index. The first term in equation (11) is referred to as the *prior*. The remainder consists of a linear combination of *constraints*, recall equation (2), with Lagrange multipliers λ^i.

Theorem 1. *The solution to the Euler-Lagrange equations for equation* (11) *can be found by A-orthogonal projection of the original image f on the linear space* V *spanned by the filters κ_i, i.e.*

$$g = \mathcal{P}_{\mathrm{V}} f = (\kappa^i, f)_A \kappa_i \ . \tag{12}$$

Here we have defined $\kappa^i \stackrel{def}{=} G^{ij}\kappa_j$ with Gramm matrix

$$G_{ij} = (\kappa_i, \kappa_j)_A \tag{13}$$

and $G^{ik}G_{kj} = \delta^i_j$.

The functional derivative of equation (11) with respect to the image g is given by (recall equation (4))

$$\frac{\delta E(g)}{\delta g} = (I + A^\dagger A)g - \lambda^i \psi_i \tag{14}$$

The solution to the corresponding Euler-Lagrange equations is formally given by

$$g = \lambda^i (I + A^\dagger A)^{-1} \psi_i = \lambda^i \kappa_i \ . \tag{15}$$

So the filter responses can be expressed as

$$c_i = (\psi_i, g)_{\mathbb{L}_2} = \lambda^j \left(\psi_i, (I + A^\dagger A)^{-1}\psi_j\right)_{\mathbb{L}_2} = \lambda^j (\psi_i, \kappa_j)_{\mathbb{L}_2} = \lambda^j (\kappa_i, \kappa_j)_A. \tag{16}$$

Consequently $\lambda^i = G^{ij}c_j$. Applying this to equation (15) leads to

$$g = \lambda^i \kappa_i = G^{ij} c_j \kappa_i = G^{ij} (\kappa_j, f)_A \kappa_i \ = (\kappa^i, f)_A \kappa_i. \tag{17}$$

This completes the proof of Theorem 1.

Theorem 1 refers to an Euler-Lagrange formalism to comply with previous work on this subject (Kanters et al., 2003; Lillholm et al., 2003; Nielsen and Lillholm, 2001). The authors do notice the linear reconstruction problem can be approached in a simpler and more elegant way. This approach is sketched in Appendix A.

3. Reconstruction from Singular Points

The theory of the previous section is applicable to any set of linear features. Here we are particularly interested in feature attributes of so-called singular points in Gaussian scale space. A Gaussian scale space representation $u(x; s)$ in n spatial dimensions is obtained by convolution of a raw image $f(x)$ with a normalized Gaussian:

$$u(x; s) \ = (f * \varphi_s)(x) \qquad \varphi_s(x) = \frac{1}{\sqrt{4\pi s}^n} e^{-\frac{||x||^2}{4s}}. \tag{18}$$

For the remainder of this paper we use the following convention for the continuous Fourier Transform

$$\mathcal{F}(f)(\omega) = \hat{f}(\omega) = \frac{1}{\sqrt{2\pi}^n} \int_{-\infty}^{\infty} e^{-i\omega x} f(x) dx$$
$$\mathcal{F}^{-1}(f)(x) = f(x) = \frac{1}{\sqrt{2\pi}^n} \int_{-\infty}^{\infty} e^{i\omega x} \hat{f}(\omega) d\omega. \tag{19}$$

Notice that with this definition Fourier transformation becomes a unitary transformation.

3.1. Singular Points

A *singular point* is a *non-Morse critical point* of a Gaussian scale space representation of an image. Scale s is taken as a control parameter. This type of point is also referred to in the literature as a *degenerate spatial critical point* or as a *toppoint* or *catastrophe*.

Definition 3 (Singular Point). A singular point $(x; s) \in \mathbb{R}^{n+1}$ is defined by the following equations,

in which ∇ denotes the spatial gradient operator:

$$\begin{cases} \nabla u(\mathbf{x}; s) = 0 \\ \det \nabla \nabla^T u(\mathbf{x}; s) = 0 \end{cases} \tag{20}$$

The behavior near singular points is the subject of *catastrophe theory*. Damon (1995) rigorously studied the applicability of established *catastrophe theory* in a scale space context. Florack and Kuijper (2006) have given an overview of the established theory in their paper about the topological structure of scale space images for the generic case of interest. More on catastrophe theory in general can be found in a monograph by Gilmore (1993).

3.2. Prior Selection

Johansen et al. (1986, 2000) showed that a one dimensional signal is defined up to a multiplicative constant by its singular points. This is probably not the case for two dimensional signals (images). It was conjectured that these points endowed with suitable attributes do contain enough information to be able to obtain a reconstruction that is visually close to the initial image (Kanters et al., 2003).

As can be seen in Figure 1 the standard linear reconstruction proposed by Kanters et al. (2003) which uses the standard $\mathbb{L}_2$-inner product, is far from optimal. The problem can be identified by determining the number of additional singular points that appear in the reconstructed image while strictly insisting on the features to hold. In case of a perfect reconstruction the number of singular points would be equal for the reconstructed and original image. In practice, however, one observes that a reconstruction like the one shown in Figure 1 on the right, has more singular points than the original image. The number of singular points in the reconstructed image can be reduced by smoothing the image (while not violating the constraints). Therefore a prior derived from the following inner product is proposed[2]:

$$\begin{aligned} (f, g)_A &= (f, g)_{\mathbb{L}_2} + (-\gamma\sqrt{-\Delta} f, -\gamma\sqrt{-\Delta} g)_{\mathbb{L}_2} \\ &= (f, g)_{\mathbb{L}_2} - (f, \gamma^2 \Delta g)_{\mathbb{L}_2} \\ &= (f, g)_{\mathbb{L}_2} + (\gamma \nabla f, \gamma \nabla g)_{\underline{\mathbb{L}_2}} . \end{aligned} \tag{21}$$

This prior introduces a smoothness constraint to the reconstruction problem. The degree of smoothness is controlled by the parameter γ. When γ vanishes the projection equals the one from standard linear reconstruction (Kanters et al., 2003). Note that this is a standard prior in first order Tikhonov regularization (Florack et al., 2004; Tikhonov and Arseninn, 1977). A visualization of the projection using the inner product of equation (21) can be found in Figure 2.

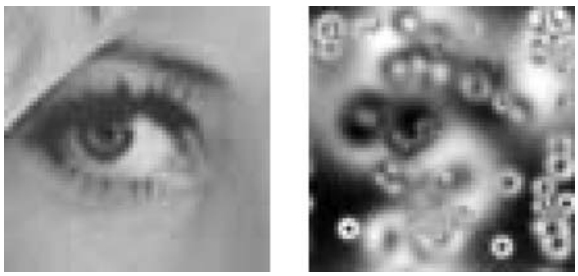

Figure 1. The image on the right hand side shows the standard linear reconstruction, taking up to second order differential structure into account, as is proposed by Kanters et al. (2003) from 63 singular points of *Lena's eye*. The original image, from which the singular points are taken is shown on the left hand side.

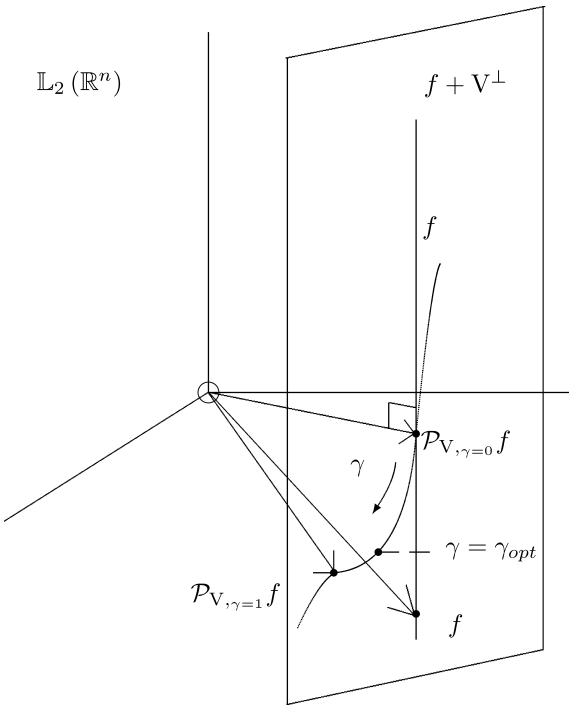

Figure 2. Illustration of the metameric class V of images with consistent features. For $\gamma = 0$ we have an orthogonal projection in $\mathbb{L}_2(\mathbb{R}^2)$. For $\gamma > 0$ this is an A-orthogonal projection, which is a skew projection in $\mathbb{L}_2(\mathbb{R}^2)$. The smoothness of the projection increases with $\gamma > 0$.

In practice one should consider

$$f \mapsto f - \overline{f}\, 1_\Omega \,, \tag{22}$$

with $\overline{f}$ the average of f and Ω denotes the support of f. Then for $A = -\gamma\sqrt{-\Delta}$

$$||f - \overline{f}||_A^2 = ||f - \overline{f}||_{\mathbb{L}_2}^2 + ||Af||_{\mathbb{L}_2}^2 \tag{23}$$

is minimized resulting in minimal variance reconstruction.

3.3. Implementation

Setting $A = -\gamma\sqrt{-\Delta}$ the A-filter equals

$$\begin{aligned}\kappa_i &= (I - \gamma^2\Delta)^{-1}\psi_i \\ &= \mathcal{F}^{-1}\left(\omega \longmapsto \frac{1}{1+\gamma^2||\omega||^2}\mathcal{F}(\psi_i)(\omega)\right). \end{aligned}\tag{24}$$

The filter shape in the spatial domain is somewhat harder to obtain. For two dimensions ($n = 2$) the convolution filter that represents the linear operator $(I - \gamma^2\Delta)^{-1}$ equals

$$\phi_\gamma(x, y) = \frac{1}{2\pi\gamma^2} K_0\left[\frac{\sqrt{x^2+y^2}}{\gamma}\right] \tag{25}$$

with K_0 representing the zeroth order modified Bessel function of the second kind. This was also noted by Florack, Duits and Bierkens (2004) who worked on Tikhonov regularization and its relation to Gaussian scale space. Notice that this kernel is singular at the origin. This is caused by the fact that a first order Sobolev space on $\mathbb{R}^2$ is not a reproducing kernel Hilbert space. By slightly increasing the order of the Sobolev space this inconvenience could be circumvented (Duits et al., 2005). The nature of the singularity is relatively harmless, however.

The calculation of the Gramm matrix G_{ij} (equation 13) is the computationally hardest part of the reconstruction algorithm. An analytic expression for this matrix is not available (unless $\gamma = 0$ (Kanters et al., 2003)). Therefore the inner products $(\kappa_i, \kappa_j)_A$ have to be found by numerical integration. By the Parseval theorem we have (recall equations (24) and (25)

$$\begin{aligned}\left(\kappa_i, \kappa_j\right)_A &= \left(\tfrac{1}{1+\gamma^2||\omega||^2}\hat{\psi}_i, \hat{\psi}_j\right)_{\mathbb{L}_2} \\ &= \left(\tfrac{1}{1+\gamma^2||\omega||^2}, \overline{\hat{\psi}}_i\hat{\psi}_j\right)_{\mathbb{L}_2} \\ &= \left(\phi_\gamma, \overline{\psi}_i * \psi_j\right)_{\mathbb{L}_2}\end{aligned}\tag{26}$$

In which ϕ_γ is given by equation (25).

At this point we have not yet specified the ψ_i filters. Since we are interested in the properties of singular points in Gaussian scale space we define the filters as follows.

Definition 4 (Feature Extraction).

A filter ψ_i is a localized derivative of the Gaussian kernel, recall equation (18), at a certain scale. Given $x, y, \xi, \eta \epsilon \mathbb{R}$ and $m, n \in \mathbb{N}_0$

$$\psi_i(x, y) \stackrel{\text{def}}{=} \frac{\partial^{m+n}\varphi_s(\xi - x, \eta - y)}{\partial x^m \partial y^n} \tag{27}$$

with $i \stackrel{\text{def}}{=} (m, n, \xi, \eta, \sigma) \in \mathbb{N}_0^2 \times \mathbb{R}^2 \times \mathbb{R}_+$.

Notice that

$$\begin{aligned}\left(\tfrac{\partial^{m+n}}{\partial x^m \partial y^n}u\right)(\xi, \eta, s) &= \left(\tfrac{\partial^{m+n}}{\partial x^m \partial y^n}\varphi_s * f\right)(\xi, \eta) \\ &= \int f(x, y)\left(\tfrac{\partial^{m+n}}{\partial x^m \partial y^n}\varphi_s\right) \\ &\quad (\xi - x, \eta - y)\, dx dy \\ &= \left(\overline{\psi}_i, f\right)_{\mathbb{L}_2} = (\psi_i, f)_{\mathbb{L}_2}\end{aligned}\tag{28}$$

since $\overline{\psi}_i = \psi_i$. So the differential structure in a point in scale space can be described by a set of linear functionals on the image f.

Applying Definition (4) to equation (26) reveals that the inner products in the Gramm matrix can be expressed as a Gaussian derivative of the spatial representation of ϕ_γ. Note that this can be exploited for any operator that one chooses to use as a regularizer.

The singularity of $\phi_\gamma(x)$ in the origin gives rise to numerical problems. The Fourier representation $\hat{\phi}_\gamma(x)$ does not have a singularity, therefore the Fourier representation of the operator is sampled and after that a discrete inverse Fourier transform is applied to it.

At this point we could construct the Gramm matrix and obtain the solution of our reconstruction problem,

according to equation (17)

$$g = G^{ij} c_j \kappa_i \ . \tag{29}$$

Instead, in order to improve accuracy, we rewrite our problem in the following manner,

$$g = \tilde{G}^{ij} \tilde{c}_j \tilde{\kappa}_i \ , \tag{30}$$

with , $\tilde{G}_{ij} = \frac{G_{ij}}{\sqrt{G_{ii}}\sqrt{G_{jj}}}$ (no summation convention), $\tilde{c}_j = \frac{1}{\sqrt{G_{jj}}} c_j$ and $\tilde{\kappa}_i = \frac{1}{\sqrt{G_{ii}}} \kappa_i$. This way the condition number of the matrix to be inverted,

$$C = \sqrt{\frac{\mu_1}{\mu_n}} \ , \tag{31}$$

with $\mu_i \geq \mu_2 \geq \ldots \geq \mu_n > 0$ its eigenvalues, can be controlled. Since the condition number solely depends on the largest and the smallest eigenvalue we can easily minimize equation (31) by setting the diagonal of this matrix to unity, as is expressed in equation (30). In matrix notation we note that (underscore denotes vectorial representation)

$$\left(S\underline{\kappa}\right)^T (SGS)^{-1} S\underline{c} = \underline{\kappa}^T G^{-1} \underline{c} \ , \tag{32}$$

where we used $S^T = S$, with

$$S_{ij} = \begin{cases} \frac{1}{\sqrt{G_{ii}}} & \text{if } i = j \\ 0 & \text{if } i \neq j \end{cases} \ , \tag{33}$$

$\underline{\kappa} = (\kappa_1, \ldots, \kappa_N)^T$ and $\underline{c} = (c_1, \ldots, c_N)^T$.

3.4. Richer Features

Obtaining a visually appealing reconstruction from singular points can be achieved by selecting an "optimal" space for projection. This approach is discussed above. Another way to enhance the quality of the reconstruction is by using more information about the points that are used for reconstruction. In the standard case only up to second order differential structure was used. In our experiments also higher order differential properties of the singular points were taken into account. This has the side effect that the Gramm matrix will be harder to invert when more possibly dependent properties are used.

4. Evaluation

To evaluate the suggested prior and the proposed reconstruction scheme reconstructions from singular points of different images are performed. The singular points are obtained using ScaleSpaceViz (Kanters, 2004), which is based on a zero-crossings method. After the singular points are found the unstable ones are filtered out by applying a threshold on the amount of structure that is present around a singular point. The amount of structure can be found by calculating the "differential quadratic total variation norm" or "deviation from flatness"

$$\text{tv} = \sigma^4 \text{Tr}\left(\mathbf{H}^2\right) \tag{34}$$

that was proposed by Platel et al. (2004). $\mathbf{H}$ represents the Hessian matrix and σ represents the scale at which the singular point appears. The reconstruction algorithm is implemented in Mathematica (Wolfram, 1991).

The images that are chosen to evaluate the performance of the reconstruction algorithm are those used by Kanters et al. (2003) and Lillholm et al. (2003) for the evaluation of their reconstruction algorithms. The size of the first image is 64×64 pixels and the size of the second image is 128×128 pixels. The pixel values of these images are integer valued ranging from 0 to 255.

4.1. Qualitative Evaluation

First we study reconstruction from singular points taking into account up to second order derivatives of the image at the locations of the singular points. Figure 3 shows the reconstruction from 31 singular points of *Lena's eye* . These points are selected using a tv-norm of 32. Note that the tv-norm scales with the square of the image range. The first image in the upper row displays the image from which the singular points were obtained. Successive images are reconstructions from these points with an increasing γ. The second image in the first row shows a reconstruction with $\gamma = 0$, which equals the reconstruction by Kanters et al. (2003), and the first picture in the second row depicts the reconstruction with a minimal relative $\mathbb{L}_2$-error. The same convention is used in the reconstruction from 55 singular points of *MR brain* that is displayed in Figure 4. The singular points of this image were acquired using a tv-norm of 128. Figure 3 shows the "fill-in effect" of the smoothing prior. The reconstruction with the

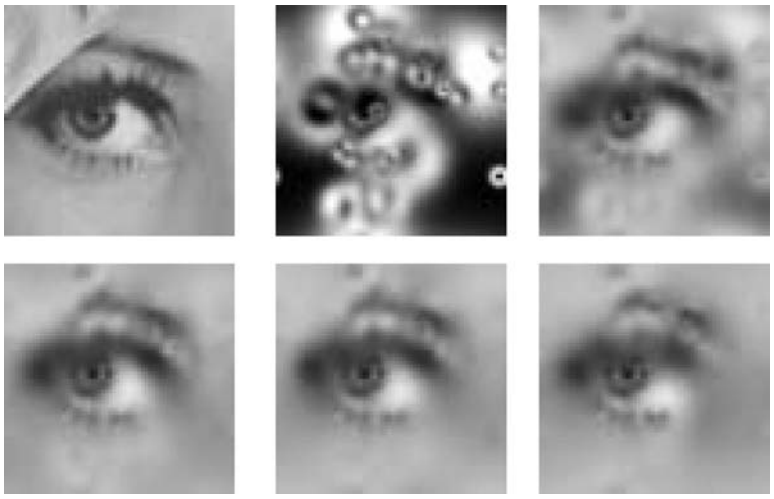

Figure 3. Reconstruction from 31 singular points of *Lena's eye* with up to second order features. The upper row shows the original image and reconstructions with $\gamma = 0$ and $\gamma = 5$. The second row shows reconstructions with $\gamma = 22$, $\gamma = 50$ and $\gamma = 250$. The first image in the second row shows the reconstruction with the lowest relative $\mathbb{L}_2$-error.

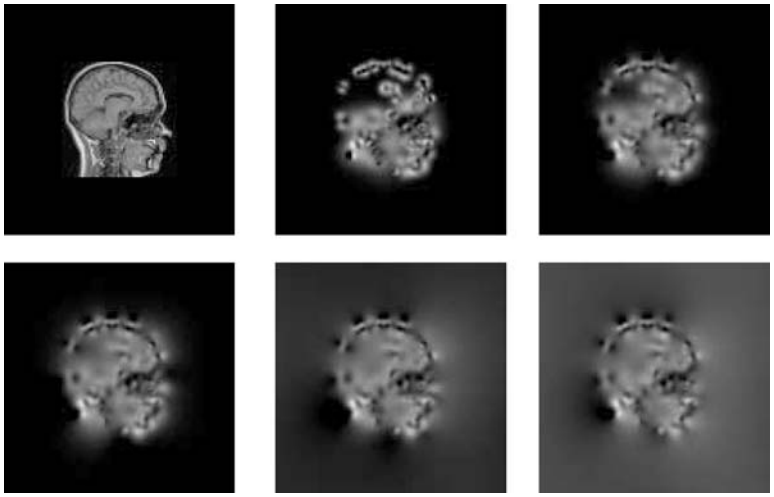

Figure 4. Reconstruction from 55 singular points of *MR brain* with up to second order features. The upper row shows the original image and reconstructions with $\gamma = 0$ and $\gamma = 3$. The second row shows reconstructions with $\gamma = 7$, $\gamma = 50$ and $\gamma = 250$. The first image in the second row shows the reconstruction with the lowest relative $\mathbb{L}_2$-error.

smallest relative $\mathbb{L}_2$-error is visually more appealing than the images with a smaller γ. A reconstruction with $\gamma = 250$ lacks details that were visible in the other reconstructions. This happens because the Gramm matrix is harder to invert when dependent basis functions are used. With an increasing γ the kernels become wider and thus more dependent on one another. The reconstructions of *MR brain* show "leaking" edges. Because the prior smoothes the image the very sharp edges of this image are not preserved and consequently the leaking effect appears.

To investigate the influence of enrichment of the features the same experiments are repeated but up to fourth order derivatives are taken into account in the features. The results for the reconstruction from the singular points of *Lena's eye* can be found in Figure 5 and the results for the reconstruction from the singular points of *MR brain* are depicted in Figure 6. In both cases the images show more detail and are visually more appealing than their second order counter parts. The reconstruction of the *MR brain* image still shows leaking but this effect is reduced when compared to second order

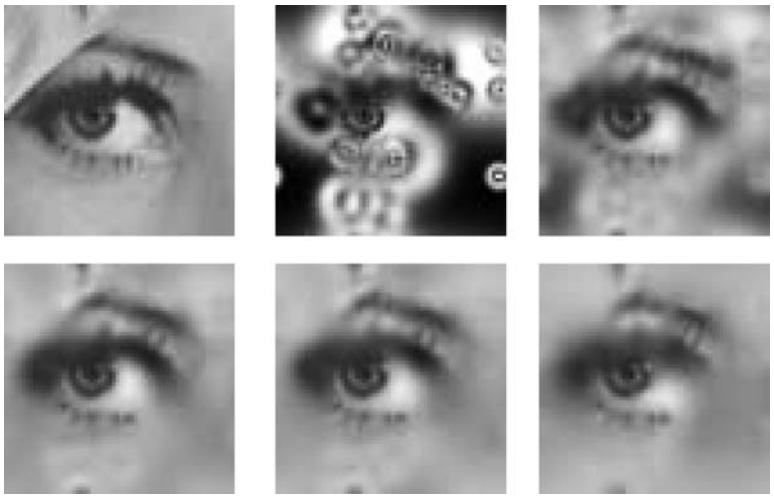

Figure 5. Reconstruction from 31 singular points of *Lena's eye* with up to fourth order features. The upper row shows the original image and reconstructions with $\gamma = 0$ and $\gamma = 4$. The second row shows reconstructions with $\gamma = 19$, $\gamma = 50$ and $\gamma = 250$. The first image in the second row shows the reconstruction with the lowest relative $\mathbb{L}_2$-error.

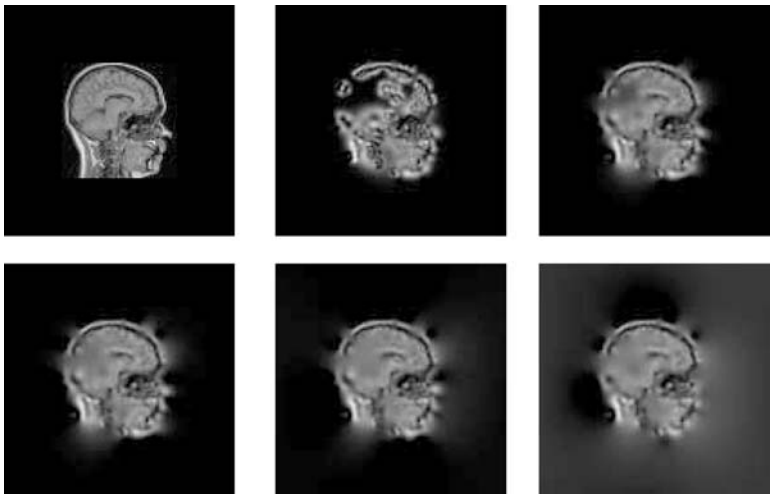

Figure 6. Reconstruction from 55 singular points of *MR brain* with up to fourth order features. The upper row shows the original image and reconstructions with $\gamma = 0$ and $\gamma = 4$. The second row shows reconstructions with $\gamma = 8$, $\gamma = 50$ and $\gamma = 250$. The first image in the second row shows the reconstruction with the lowest relative $\mathbb{L}_2$-error.

reconstruction. Inspection of Figures 3,4,5 and 6 shows that, although the reconstructions are still far from optimal, remarkably few singular points are involved relative to the total number of pixels.

4.2. Quantitative Evaluation

In order to verify the quality of the reconstructions of both images under a varying γ the relative $\mathbb{L}_2$-error,

$$\mathbb{L}_2\text{-error} = \frac{||f - g||_{\mathbb{L}_2}}{||f||_{\mathbb{L}_2}}, \tag{35}$$

of the reconstructed images is calculated. Figure 7 shows four graphs depicting this error for both second order and fourth order reconstruction of *Lena's eye* and *MR brain*. All graphs show that an optimal value exists for the γ parameter. This can be explained by the fact that the Gramm matrix is harder to invert with increasing γ due to increasing correlation among the filter cf. equation (26). Because of that dependent equations will be removed during the Singular Value Decomposition, which is used to obtain the inverse of the Gramm matrix. This leads to a reconstruction with less detail

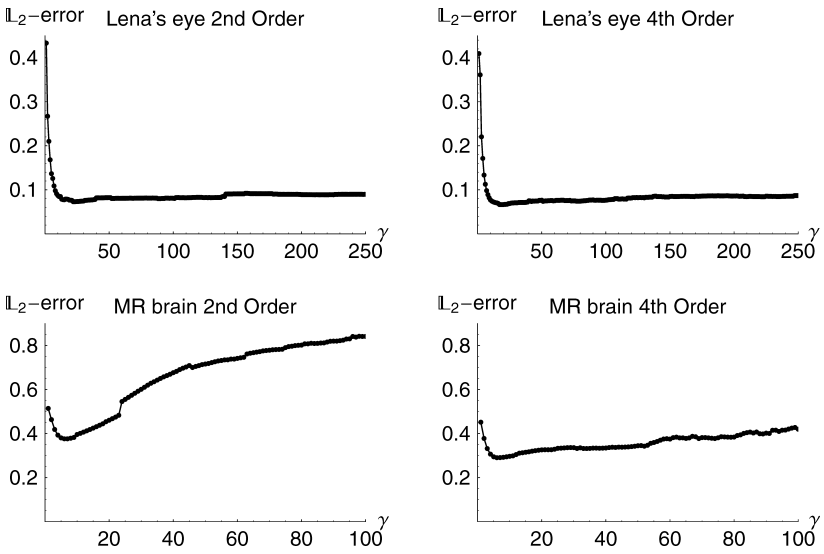

Figure 7. The relative $\mathbb{L}_2$-error of the reconstructions from 31 singular points of *Lena's eye* (upper row) and 55 singular points of *MR brain* (lower row). The first column shows the $\mathbb{L}_2$-error for varying γ when second order reconstruction is used, i.e. up to second order derivatives are taken into account in the features. The second column displays fourth order reconstruction. The minimal relative $\mathbb{L}_2$-errors of the reconstructions of *Lena's eye* ($\gamma = 22$ and $\gamma = 19$) are larger than those of *MR brain* ($\gamma = 7$ and $\gamma = 8$). This suggests, in order to reduce the "fill-in effect" that causes this difference for the optimal value of γ, the use of anisotropic diffusion (which will be addressed in future work).

and thus a larger $\mathbb{L}_2$-error. The reconstructions of the *MR brain* image show an increasing $\mathbb{L}_2$-error with an increasing γ. This error becomes even larger than the $\mathbb{L}_2$-error of the reconstruction with $\gamma = 0$. This can be attributed to the sharp edges of the head that are smoothed and thus show leaking into the black surroundings of the head. The background clearly dominates the contribution to the $\mathbb{L}_2$-error. The reconstruction of *Lena's eye* does not suffer from this problem because of its smoothness.

5. Conclusions and Recommendations

We proposed a linear reconstruction method that leaves room for selection of arbitrary priors as long as the prior is a norm of Sobolev type. This greatly reduces the complexity of the reconstruction algorithm compared to non-linear methods.

We select one possible prior characterized by a free parameter γ that aims for a smooth reconstruction. This provides a control parameter for selecting different metameric reconstructions, i.e. reconstructions all consistent with the prescribed constraints. Comparisons with standard linear reconstruction as done by Kanters et al. (2003) show it is possible to improve the reconstruction quality while retaining linearity. Reconstruction from a selection of singular points of the *MR brain* image proves to be more difficult than reconstruction of smoother images like *Lena's eye*. The problem, that shows up as "leaking" edges, is reduced by taking higher order differential structure into account in the reconstruction algorithm. When the γ parameter is increased basis functions get more dependent on each other. This leads to a harder to invert Gramm matrix and consequently to a reduction of detail in the reconstruction.

Both, taking a $\gamma > 0$ and taking higher order features into account, lead to visually more appealing images and a smaller $\mathbb{L}_2$-error when comparing with standard linear reconstruction. It remains an open question how to select an optimal γ.

Future work will include the use of anisotropic diffusion depending on the local image orientation and investigation of so called flux features. Additionally other priors that fit in the proposed framework will be investigated.

Acknowledgement

The Netherlands Organisation for Scientific Research (NWO) is gratefully acknowledged for financial support.

A. Simple Alternative Approach to Theorem 1

Recall that V is the span of the filters κ_i. Then

$$V^{\perp} = \{f \in \mathbb{L}_2(\mathbb{R}^2) \mid (\kappa_i, f)_A = 0 \; \forall i = 1, \ldots, N\} \tag{36}$$

On the space of images $\mathbb{L}_2(\mathbb{R}^2)$ we define the following equivalence relation:

$$f \sim g \Leftrightarrow (\kappa_i, f)_A = (\kappa_i, g)_A \; \forall \, i = 1, \ldots, N \; , \tag{37}$$

i.e. two images are equivalent if they share the same set of features. As a result the equivalence class $[f]$ of representant f is given by

$$[f] = \{g \in \mathbb{L}_2(\mathbb{R}^2) \mid f \sim g\} = f + V^{\perp} \; . \tag{38}$$

Next we show that the unique element g within $[f]$ that minimizes the energy $E[g] = \|g\|_A^2$ is given by the A-orthogonal projection of f on V, $\mathcal{P}_V f$:

$$\begin{aligned} \min_{g \in [f]} \|g\|_A^2 &= \min_{g \in [f]} \|g - \mathcal{P}_V f + \mathcal{P}_V f\|_A^2 \\ &= \min_{g \in [f]} \|g - \mathcal{P}_V f\|_A^2 + \|\mathcal{P}_V f\|_A^2 \end{aligned} \tag{39}$$

and this equals $\|\mathcal{P}_V f\|_A^2$ only in the case $g = \mathcal{P}_V f$. Notice with respect to the last equality (equation (39)) the Pythogoras theorem has been used, which can be applied since $(g - \mathcal{P}_V f) = (g - \mathcal{P}_V g) \in V^{\perp}$ and $\mathcal{P}_V f \in V$.

Notes

1. By Neumann (Yosida, 1980 p. 200), we have that for every closed densely defined operator A in a Hilbert space $\mathcal{H}$ the operator A^*A is self adjoint and $(I + A^*A)$ has a bounded inverse.
2. The operational significance of the fractional operator $-\sqrt{-\Delta}$, which is the generator of the Poisson scale space, is explained in detail by Duits et al. (2004). In Fourier space it corresponds to the multiplicative operator $-||\omega||$.

References

Damon. J. 1995. Local Morse theory for solutions to the heat equation and Gaussian blurring. *Journal of Differential Equations*, 115(2):368–401.

Remco Duits. 2005. *Perceptual Organization in Image Analysis*. PhD thesis, Technische Universiteit Eindhoven.

Duits R., Florack L., ter Haar Romeny, B. and de Graaf. J. 2004. On the axioms of scale space theory. *Journal of Mathematical Imaging and Vision*, 20:267–298.

Duits, R., Janssen, B.J., Kanters, F.M.W. and Florack, L.M.J. 2005. Linear image reconstruction by means of inner products of sobolev type. In *The first International Workshop on Deep Structure, Singularities and Computer Vision*. Springer.

Florack, L., Duits, R. and Bierkens, J. 2004. Tikhonov regularization versus scale space: A new result. In *Proceedings of the 11th International Conference on Image Processing (Singapore, 24–27)*, pages 271–274.

Florack, L. and Kuijper, A. 2000. The topological structure of scale-space images. *Journal of Mathematical Imaging and Vision*, 12(1):65–79.

Gilmore, R. 1981. *Catastrophe Theory for Scientists and Engineers*. Dover Publications, Inc., New York, 1993. Originally published by John Wiley & Sons, New York.

Johansen, P., Nielsen, M. and Olsen, O. F. 2000. Branch points in one-dimensional gaussian scale space. *Journal of Mathematical Imaging and Vision*, 13(3):193–203.

Johansen, P., Skelboe, S., Grue, K. and Andersen, J. D. 1986. Representing signals by their top points in scale-space. In *Proceedings of the 8th International Conference on Pattern Recognition (Paris, France, 1986)*, IEEE Computer Society Press, pp. 215–217.

Kanters, F.M.W., Platel, B., Florack L.M.J. and ter Haar Romeny, B.M. 2003. Image reconstruction from multiscale critical points. In Lewis Griffin and Martin Lillholm, editors, *Scale Space Methods in Computer Vision, 4th International Conference, Scale Space 2003*, Isle of Skye, UK, Springer, pp. 464–478.

Kanters, 2004. Scalespaceviz. F.M.W. http://www.bmi2.bmt.tue.nl/image-analysis/people/FKanters/Software/ScaleSpaceViz.html.

Kybic, J., Blu, T. and Unser. M. 2002. Generalized sampling: a variational approach – part I: Theory. *IEEE Transactions on Signal Processing*, 50:1965–1976.

Kybic, J., Blu, T. and Unser, M. 2002. Generalized sampling: a variational approach – part II: Applications. *IEEE Transactions on Signal Processing*, 50:1965–1976.

Lillholm, M., Nielsen, M. and Griffin. L. D. 2003. Feature-based image analysis. *International Journal of Computer Vision*, 52(2/3): 73–95.

Nielsen, M. and Lillholm, M. 2001. What do features tell about images? In M. Kerckhove, editor, *Scale-Space and Morphology in Computer Vision: Proceedings of the Third International Conference, Scale-Space 2001, Vancouver, Canada*, volume 2106 of *Lecture Notes in Computer Science*, Springer-Verlag, Berlin, pp. 39–50.

Papoulis, A. 1977. Generalized sampling expansion. *IEEE Transactions on Circuits and Systems*, 24:652–654.

Platel, B., Kanters, F.M.W., Florack, L.M.J. and Balmachnova, E.G. 2004. Using multiscale top points in image matching. In *Proceedings of the 11th international conference on Image Processing*, pp. 389–392.

Shannon. C.E. 1949. Communication in the presence of noise. In *Proc. IRE*, vol. 37, pp. 10–21.

Tikhonov, A. and Arseninn, V. Y, 1977. *Solution of Ill-Posed Problems*. John Wiley & Sons, New York.

Unser, M. and Aldroubi, A. 1994. A general sampling theory for nonideal acquisition devices. *IEEE Transactions on Signal Processing*, 42:2915–2925.

Wolfram, S. 1991. *Mathematica: A System for doing Mathematics by Computer*. Addison-Wesley, second edition.

Yosida. K. 1980. *Functional Analysis*. Springer-Verlag, Berlin, sixth edition.